



RESEARCH LETTER

10.1029/2022GL100170

Key Points:

- Seismic sensing of valley confined floods improves classic detection approaches
- Near-real time information on flood magnitude, trajectory, and velocity
- Gate keeper seismometer networks can improve flood risk management in Europe

Supporting Information:

Supporting Information may be found in the online version of this article.

Correspondence to:

M. Dietze,
michael.dietze@uni-goettingen.de

Citation:




Dietze, M., Hoffmann, T., Bell, R., Schrott, L., & Hovius, N. (2022). A seismic approach to flood detection and characterization in upland catchments. *Geophysical Research Letters*, 49, e2022GL100170. <https://doi.org/10.1029/2022GL100170>

Received 27 JUN 2022
 Accepted 29 SEP 2022

Author Contributions:

Conceptualization: M. Dietze, T. Hoffmann
Data curation: R. Bell
Formal analysis: M. Dietze, T. Hoffmann, R. Bell
Investigation: M. Dietze, R. Bell, L. Schrott, N. Hovius
Methodology: M. Dietze
Software: M. Dietze
Writing – original draft: M. Dietze, T. Hoffmann, R. Bell, L. Schrott, N. Hovius
Writing – review & editing: M. Dietze

A Seismic Approach to Flood Detection and Characterization in Upland Catchments

M. Dietze^{1,2} , T. Hoffmann³ , R. Bell³, L. Schrott³, and N. Hovius^{2,4} 

¹Georg-August-University Göttingen, Faculty of Geosciences and Geography, Göttingen, Germany, ²GFZ German Research Centre for Geosciences, Section 4.6 Geomorphology, Potsdam, Germany, ³University of Bonn, Department of Geography, Bonn, Germany, ⁴University of Potsdam, Institute of Geosciences, Potsdam, Germany

Abstract About 10% of Europe's surface area is prone to rapid flooding of rivers confined in valleys. The devastating potential of such floods is exacerbated by the deficits of existing gauging networks, including low station densities and recording frequencies, and lack of information beyond stage height. Here, we use seismic data of the July 2021 Ahrtal flood, Germany, to extract information to complement sparse hydrometric data, and to reconstruct the rapid evolution of this fatal event. We show that a seismic station can deliver essential flood metrics such as magnitude, propagation velocity and debris transport rate. These seismic products provide high resolution insight to the non-linear flood behavior. We argue that an approach combining distributed low-cost seismometers with existing seismic stations, can provide important real time data on future catastrophic floods and associated hazards in upland catchments, offering precious response time also in currently ungauged landscapes.

Plain Language Summary Rapidly evolving floods are a major hazard for 10% of European landscapes. They are hard to adequately detect and describe by the classic gauge station scheme, but seismic sensors provide a valuable alternative to this difficulty. A seismometer can sense a flood like the devastating one that hit the Ahr valley, Germany, in July 2021 up to 1.5 km away. The seismic footprint of the flood allows to provide information on flood magnitude, velocity and trajectory at sub-minute resolution and at near real time. We show how this new approach can be utilized for future flood protection.

1. Introduction

River floods are a major hazard, especially in narrow upland valleys that cover up to 10% of Europe (cf. Supporting Information S1). While Alpine communities are commonly tuned to this hazard, awareness is lower in other upland regions (Schneiderbauer et al., 2021). There, floods are typically thought to be associated with larger rivers (fluvial floods), with day long warning times and inundation damage by high water levels. Under a warming climate with higher atmospheric moisture concentrations and more frequent stationary pressure fields (IPCC, 2018; Nikogosian et al., 2021), European upland regions have already been but will become increasingly exposed to persistent strong precipitation that may cause hazardous floods in smaller catchments (pluvial floods). Communities in such catchments require efficient and reliable flood warning.

Existing hydrometric station networks, even dense ones in economically strong countries, are not designed to adequately anticipate, track and characterize rapidly evolving floods in catchments of 10¹–10² km². The majority of stream gauges measure only one metric: water level, and do so once in 15 min. With tens of km between stations on a stream, estimates of flood propagation speed have a time delay of an hour at best and are not available for the valley segment upstream of the first station. Moreover, water levels may well rise by up to a meter between stage measurements, and in-stream gauging stations are inherently prone to intra-flood erosion and deposition effects (Cook et al., 2018) as well as destruction by floodwater or the coarse debris it transports. Often this debris and the accompanying sediment load add substantially to the damage caused by flood water alone.

The destructive power of rapidly evolving floods was evident on 14–15 July 2021, after a stationary atmospheric low had discharged up to 250 mm of rain within three days in the Eifel upland region of Germany (Junghänel et al., 2021). The uplifted Eifel plateau is dissected by steep and narrow valleys, feeding the headwaters of several larger rivers. The 900 km² catchment of the Ahr River, a tributary of the Rhine, experienced a fast rising flood with peak discharge estimates at 1,200 m³/s (Roggenkamp & Herget, 2022) inundating parts of 15 towns,

© 2022. The Authors.

This is an open access article under the terms of the [Creative Commons Attribution License](https://creativecommons.org/licenses/by/4.0/), which permits use, distribution and reproduction in any medium, provided the original work is properly cited.

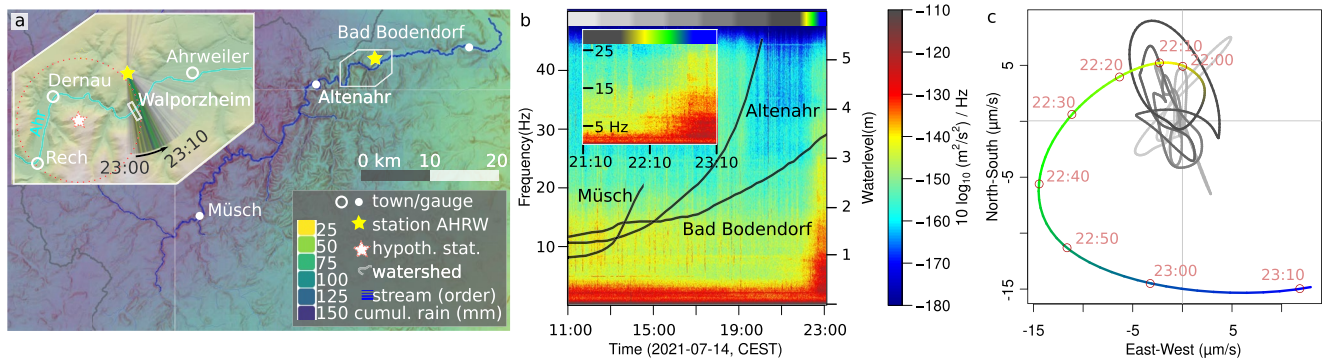


Figure 1. Flood affected Ahrtal and the seismic imprint of the flood. (a) Topography and precipitation intensity (12–15 July 2021 72 hr sum). Inset shows reach where the Ahr enters a wide valley. Color graded lines depict azimuth of seismic polarization analysis, colors according to legend in (b). White rectangle shows spatial coverage of inundation map in Figure 2b Spectrogram recorded at station AHRW with available hydrographs. Inset shows last 2 hours of seismic data. (c) Horizontal seismic particle motion trajectory at station AHRW (color as in b).

affecting 42,000 people and killing 134 (Bell et al., 2022; Dietze & Ozturk, 2021). This is the highest number of fatalities by a natural hazard in Germany since 1962.

Three hydrological stations operated along the 85 km long Ahr River (Figure 1a, Supporting Information S1), and further stations in mostly the southern tributaries that typically contributed most of the discharge during previous floods. On 14 July 2021, the gauge in Müsch (river km 63) recorded a progressive water level rise from 13:00 CEST until its failure around 15:00. The gauge at Altenahr, 32 km downstream of Müsch, was destroyed just after 19:15 while the water level was still rising exponentially. An hour before that failure, state authorities issued a water level correction, from more than 5 m back to 4 m. Soon after the water levels did indeed reach the 5 m level, destroying the gauge. They continued to rise to at least 6.9 m around 20:24 and a maximum level of more than 9 m (Bell et al., 2022). This non-linear increase paired with the lack of information about any of these dynamics left decision makers essentially blind folded.

Cross-correlation analysis of the hydrographs from Müsch and Altenahr (Supporting Information S1) yielded a time lag of 5.75 hr (cross-correlation coefficient $r = 0.7$) and hence an average flood propagation speed of about 1.5 m/s. The station at Bad Bodendorf, 27 km farther downstream had a time lag of 6.75 hr relative to Altenahr ($r = 0.7$), implying a flood velocity of 1.1 m/s. Applying this velocity, we estimate that the fast rising limb (Figure 1b) of the flood arrived at Ahrweiler, 15 km downstream from Altenahr around 22:30. However, such calculations can only be made in hindsight, and do not provide a solid basis for adequate early warning. Furthermore, the water level in Bad Bodendorf started to rise earlier because that reach also collected discharge from other contributing channels, resulting in some further non-linearity. To improve the anticipation of a rapidly developing flood, more detailed information is required, at the least information about water level and flood propagation velocity, both at significantly higher frequency than 15 min. Preferably, information is also available about large debris in the flooding river, such as large woody material, swept up vehicles and fragments of collapsed buildings.

Seismometers installed at safe distance from flooding river channels are sensitive to several flood parameters such as water level, discharge, and event propagation velocity (Cook et al., 2018, 2021; Goodling et al., 2018; Yang et al., 2018). They record ground motion signatures of river processes like turbulence-driven force fluctuations and bedload particle impacts on the river bed, superimposed on numerous other seismic signals. Disentangling this information may yield scaled time series of flood properties. Here, we use data from a seismic station of the German Regional Seismic Network (FDSN code GR), located in the Ahr catchment near Ahrweiler (station AHRW in Figure 1a), to gain deeper insights into the 2021 Ahrtal flood and to probe the potential for seismically based flood warning in ungauged upland catchments.

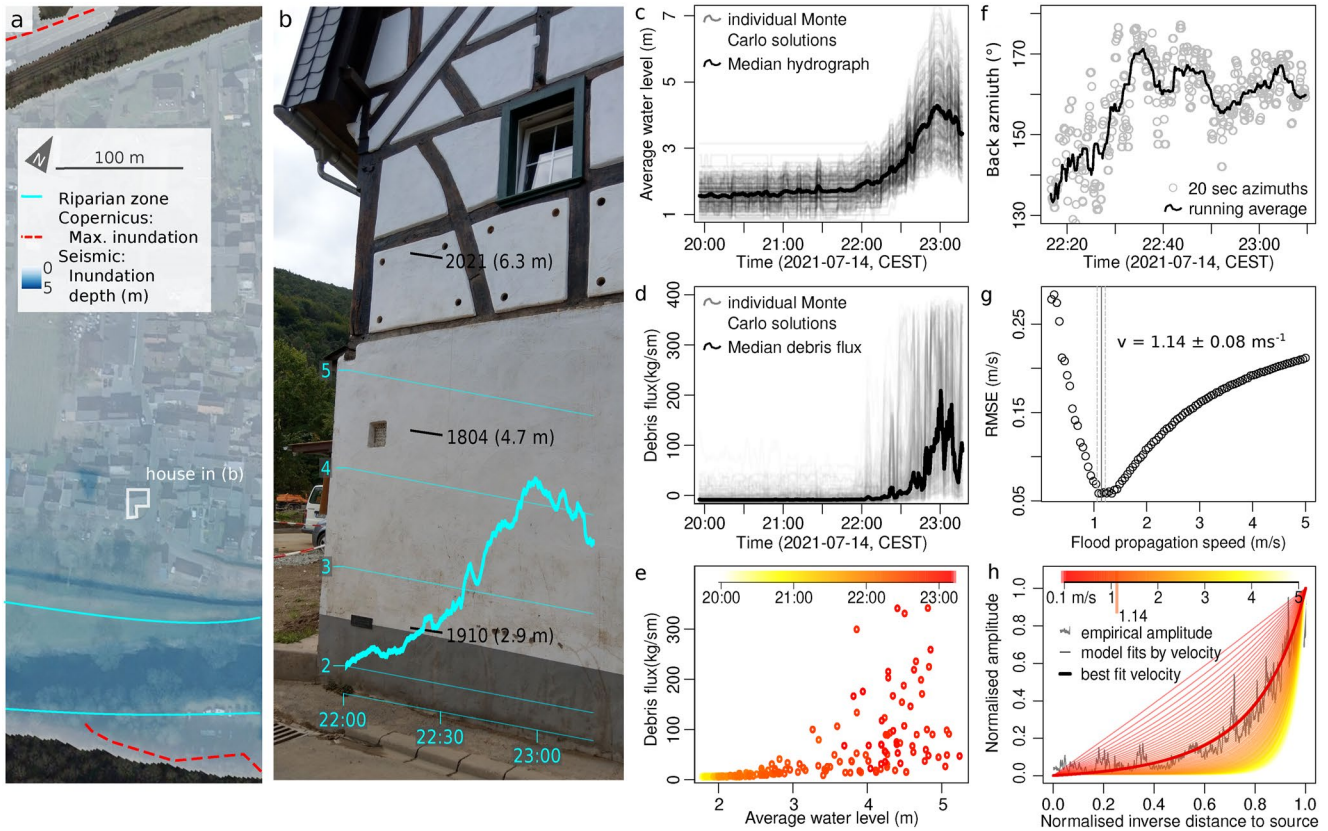


Figure 2. Seismic flood information. (a) Swath from station AHRW to the closest point on the Ahr River with posterior inundation mapping (red dashed line) and inundated area at maximum seismic inversion water level (DEM-based surface elevation below seismically predicted water level). For wider spatial context see Figure 1b House in Walporzheim with recent and historic flood marks and perspective plot of the seismically estimated water level above the river bed, not corrected for stream bed aggradation and effects of flow obstruction by densely spaced buildings. (c) Hydrograph from seismic inversion. (d) Debris flux from seismic inversion. (e) Nonlinear relationship between water level and debris flux. (f) Angle of source incidence to station AHRW. (g) RMSE values of different flood propagation velocity estimates with >95% best fit value range indicated as mean (solid line) and standard deviation (dashed line). (h) Fits of empirical seismic signal envelope with different flood propagation velocities.

2. Materials and Methods

For a seismic synopsis, particle motion analysis was performed for the time period 2021-07-14 10:00:00 to 22:10:00 UTC. The raw seismic data with 100 Hz sampling frequency, downloaded via FDSN data services were deconvolved, low pass filtered at 0.0001 Hz (Yang et al., 2018) and plotted on the horizontal plane. The seismic spectrogram was calculated from the unfiltered signal for the same time interval, using a 30 s window with 80% overlap, smoothed by a 15 s subwindow also with 80% overlap. Polarization analysis was performed for the period 2021-07-14 21:00:00 to 22:10:00 UTC on deconvolved, 1–4 Hz bandpass filtered seismic data in 20 s long 75% overlapping windows. The azimuths (Figure 2f) were smoothed with a five sample running median filter and also with a 50 sample running median filter. Statistical descriptions of the azimuth were calculated as mean and standard deviation for the intervals 21:00:00–21:45:00 and 21:45:00–22:09:30 UTC.

Inversion of the seismic spectra for water level and debris flux were processed using the approach of Dietze et al. (2019), which is based on physical models for turbulence (Gimbert et al., 2014) and bedload transport (Tsai et al., 2012), extended by a new, outer Monte Carlo loop to account for further parameter uncertainty. For a full description and justification of the ranges of model parameters see Supporting Information S1. Water level was allowed to range between 0.6 and 10 m, debris flux between 0 and 400 kg/sm. Specific sediment density was set to 2650 kg/m³, river gradient to 0.025, and the distance from the seismometer AHRW to the channel to 1,100 m. The inversion was done for the most energetic frequency range 1–8 Hz. The remaining parameters were allowed to randomly range between to following limits: median grain size 0.05–0.30 m, ground quality factor 30–50, Rayleigh phase wave velocity 500–800 m/s, wave velocity variation exponent ± 0.1 and Greens Function

displacement amplitude parameters 0.6 and 1.0. In each of the 500 Monte Carlo loops using one of the randomly and fixed assigned model parameters, we calculated 500 reference sets and resulting reference spectra and identified the best fits to the empirical data, to retrieve the respective water level and debris flux curves. From all 500 running median curves (5 sample window size), we calculated the compound median curves for plotting. As an independent test, the water level based bedload flux was calculated with the revised Meyer-Peter & Müller equation (Wong & Parker, 2006), using the seismically constrained water level curve as described above. Spectral prediction of sensor ranges for hypothetical deployment sites was performed using the turbulence and bedload flux models of the inversion approach, applying the maximum water level and debris flux values from the inversion described above.

Flood propagation velocity modeling was performed using the approach of Burtin et al. (2016), testing velocity values between 0.1 and 5 m/s on the 20 s running mean smoothed, deconvolved and 5–40 Hz band pass filtered seismic envelope between 20:10:00 and 21:40:00 UTC. As seismic ground property parameters we used the mean values of the inversion parameter ranges as reported above.

To estimate the total area of flood prone, valley confined landscapes in Europe, we performed a 30 m digital elevation model analysis. We identified flood prone valley confined landscapes as areas that have a minimum local relief of 50 m (implying sufficiently high valley slopes) within a 984 m large radius (radius defined by DEM grid size, for data sources see Supporting Information S1), a minimum drainage area of 10 km² (alternatively 1 km², not discussed in main text but see Supporting Information S1 for details) and a maximum drainage area of 900 km² (size of the Ahr catchment, see Supporting Information S1 for discussion on minimal effect of larger areas). Boolean combination of these three criteria yielded a European map from which we extracted the cumulative classified pixel area.

3. The Seismic Flood Footprint

During the Ahrthal flood, station AHRW recorded data until grid power cut out at 23:19 on 14 July. The spectrogram of AHRW (Figure 1b) shows constant seismic power around 2 Hz, which is likely caused by the turbulent flow of the Ahr at a water level of <1 m. With the advancing flood, seismic power rose in all frequency bands by a factor 300, most conspicuously between 2 and 15 Hz, similar to what has been observed in mountain valley floods (Cook et al., 2018; Coviello et al., 2018). It is very unlikely that a non-fluvial process could have generated these specific frequency characteristics and temporal evolution patterns during the flood.

While the flood was still far from station AHRW, seismic particle motion at the station was mainly around the coordinate origin (Figure 1c). Starting at 22:10, the trajectory systematically moved toward the southwest for 30 min before veering to the southeast and then the east during the remaining 30 min of record time. The degree of polarization rises from around 0.28 to 0.49 during that time. We attribute this pattern of systematic particle motion, which was not recorded at other seismic stations in the region (Supporting Information S1), to surface tilt due to a large, mobile mass, approaching the station from the southwest, passing it to the south and then moving off toward the east. Other studies (Yang et al., 2018) have reported a similar tilt signal due to the surface load of a flooding river at several km distance. Hence, a clear tilt trajectory can be a first order indicator of a propagating flood (Figure 1c), if it evolves progressively over time, the source moves along a channel and is within a sensible distance of the seismometer, and the pattern is not visible at other stations outside the sensitive range. Thus, spectrogram and particle motion analysis allow first order qualitative insight, useful for flood early detection and warning, while further insight into the event characteristics requires additional analysis.

4. Insight to Flood Kinetics

Previous seismic investigations of large, debris carrying events (Cook et al., 2018, 2021; Eibl et al., 2017; Walter et al., 2017) have found that a distinct signal is generated by the fast-rising limb of a flood, which allows event tracking and quantification. Using the seismic data from station AHRW of the rising limb of the 2021 Ahrthal flood, we have attempted to quantify flood magnitude, that is, water level, flood propagation velocity and the amount of transported debris.

Flood magnitude can be estimated using the dependence of seismic turbulence signals on flow depth, as well as the ground motion caused by impact of mobilized solid particles on the flood bed (Dietze et al., 2019; Gimbert

et al., 2014; Polvi et al., 2020; Tsai et al., 2012). Our Monte Carlo based inversion results were computationally efficient: 7.8 ms per 30 s long time slice, that is, 3.9 s for 500 Monte Carlo loops on consumer grade laptop using a single CPU. They show an initial average water level of the Ahr near Ahrweiler of less than 2 m. In the evening, the water level progressively increased, more rapidly from about 22:00, peaking at 4.2 m just before 23:00, before slowly falling during the final minutes of the AHRW record. This seismic estimate is 2.1 m below the highest flood marks on houses in Ahrweiler, the town nearest to station AHRW (Figures 2a and 2b), where the flood reached maximum water levels some hours later. Clogging and eventual destruction of 62 out of 75 bridges along the Ahr led to a non-linear, pulsed evolution of the flood, as also reported by eye witnesses (Dietze et al., 2022). Hence, the non-stationary inverted water level may be an empirical expression of this non-linearity. Alternative reasons can be intra-event channel bed aggradation or flow obstruction by closely spaced houses, altogether possible scenarios that cannot be deciphered with only one seismic station available.

In contrast to the narrow uncertainty range of inverted water level, the scatter of possible model solutions is much larger for debris flux (Figure 2d). For the 2 hours before the significant water level rise, average debris flux values were poorly constrained, but likely below 10 kg/sm. Apparently, particles impacting the bed were not mobile yet or did not generate a seismic signal powerful enough to be recorded a kilometer away. However, in the last hour of the seismic record, relative uncertainty in debris flux inversion decreased as the average model values rose to up to 220 kg/sm. With data from a single station it is not possible to determine whether individual peaks in the curve indicate discrete pulses debris transport (Polvi et al., 2020) or a change in hydraulic channel geometry (Cook et al., 2018). Regardless, the seismic debris flux estimates are in agreement with independent, water level-derived models (Wong & Parker, 2006) (Supporting Information S1). The time series of water level and debris flux do not evolve in a linear way (Figure 2e), highlighting the complexity of the seismic signal caused by a massive turbulent flow interacting with river bed conditions changing in space and time, and distributed infrastructure.

To estimate flood propagation, we used a single sensor amplitude modeling approach (Burtin et al., 2016). The best fits were achieved with propagation velocities of 1.14 ± 0.08 m/s (fits above 95th percentile, Figure 2g), which is consistent with the gauge-based average value of 1.1 m/s for the river segment between Altenahr and Bad Bodendorf. Our modeling, which resolves flow velocity in 30 s increments, suggests that flood arrival times and derived hydrodynamic metrics (Kreibich et al., 2009) at different settlements can be determined and communicated in near-real time.

Where a regional instrument network is in place, tracking of fast moving floods is feasible. Having data from just one station, we were limited to a polarization analysis (Goodling et al., 2018; Yang et al., 2018) (Figure 1a, inset; Supporting Information S1). For most of the time until 22:30, the azimuth of seismic waves recorded at AHRW scattered randomly between 100 and 180° ($\sigma = 37^\circ$). However, at 22:35 the azimuth focused around $161 \pm 7^\circ$, pointing to a strongly curved, eroded outer bank of the Ahr River near the entry of a wide valley section near Walporzheim (Supporting Information S1). This outer bank may have generated powerful eddies that dominated the seismic signal once the flood arrived at that location.

5. Toward Real Time Flood Anticipation

It was possible to extract essential information on an evolving upland valley flood from data recorded at a single seismic station set up for earthquake seismology, located at about 1 km from the flooding channel. If available in real time, this information could have aided impact anticipation and evacuation and rescue efforts by addressing questions such as: Which water level is to be expected (Figure 2c)? Which parts of settlements are likely to be inundated (Figure 2a)? How much debris does the flood transport (Figure 2d)? How fast does the water flow (Figure 2g)? Where is the flood front at a given time (Figure 2f)? The precision and resolution of answers to these questions would increase significantly with the number of available seismic stations in a catchment.

The rain driven July 2021 flood caused a total damage of 33 Billion € (Bell et al., 2022), predominantly in the 900 km² Ahr catchment. The benefits of early flood warning can be significant, through reduction of fatalities and damage. Currently, large scale international initiatives on flash flood early warning capabilities mainly rely on now-casting of high resolution precipitation data, propagated to physically based hydrological models to estimate possible impacts and inform trained agents for rapid warning and mitigation actions (HRC, 2007). Previous work indicates that in European flood affected catchments (Gocht et al., 2009) warning times of 12 hr can result in up to 65% risk reduction, 6 hr—the flood propagation time between subsequent Ahrtal gauges—would yield a 50%

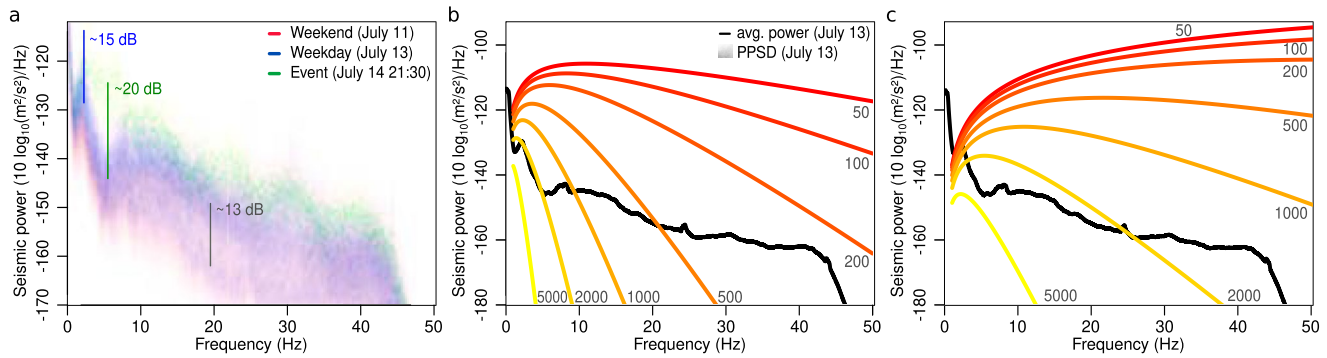


Figure 3. Seismic background and theoretical spectra of floods recorded at different distances to the channel. (a) Probabilistic power spectral density estimates of the Sunday (red shading) and Tuesday (blue shading) before the flood (green shading, only using the time interval from Figure 1b). The flood turbulence caused 15 dB power increase around 2 Hz, and the debris transport caused 20 dB power increase around 6 Hz (b) Seismic power due to turbulence for different distances to a seismic station. (c) Seismic power due to debris transport for different distances to a seismic station.

reduction. Seismic methods can support warning in ungauged catchments and contribute significantly to optimization of warning in upland catchments equipped at present only with hydrometric stations.

Catastrophic flood events (Chmiel et al., 2022; Cook et al., 2018, 2021) may involve processes that are not captured by the models of Tsai et al. (2012) and Gimbert et al. (2014), such as local erosion and deposition causing transient water level changes, or concurring hillslope and bank sediment activation. Thus, the inverted time series of water level and debris flux should be interpreted with care. That said, there are no straightforward approaches to and hence no empirical data on such additional processes in the Ahrtal case. The only information on flood magnitude was provided by mapping of peak discharge marks (Roggenkamp & Herget, 2022) or may be yielded by posterior hydrodynamic modeling, both using a series of assumptions that are as poorly rooted in event dynamics as the seismic approach.

Our approach is not restricted to the specific case of the Ahrtal. Rather, it is a generic tool, in principle applicable anywhere in comparable topographic settings. Although the inversion relies on a series of site specific parameters, those parameters can to first order be considered stable through time. Hence, they only need to be estimated once to calibrate the model, and this calibration does not rely on catastrophic events. The fluvial signature is already visible during comparably low flow conditions (Figure 2c), and a few months long calibration phase of paired seismic and hydraulic monitoring would be sufficient to constrain all relevant variables of the inversion routine.

Limits to seismic flood detection are strongly controlled by the relative strength of the flood signal with respect to the seismic noise level. In our Ahrtal example, the detection range was about 1.5–2.0 km or about 22–29 min for a flood moving at 1.14 m/s (Figures 1b, 1c, and 2f). Predictive modeling of water turbulence (Figure 3b) shows that the flood signature is drowned out by the average background noise at distances greater than 2 km. The background noise level can be reduced by picking an appropriate location that balances the distance to unwanted noise sources and the proximity to the river. While a location too far from the river would yield poor flood detection results, so will a location too close, because the turbulence spectrum of the river under normal discharge conditions will obscure the seismic signature of an approaching flood at distance. Figure 3 shows that in the case of the Ahrtal flood, at 1,100 m distance to the main channel, the noise floor in the frequency range of interest for flood detection (1–15 Hz) is dominated by the turbulence signal of the Ahr with a flow depth of about 75 cm at that time (gauge Altenahr, see Supporting Information S1).

Optimization of seismic station location can bring significant detection improvements. A hypothetical station located 2 km southwest of the site of AHRW would have a 2 km detection range for the July 2021 flood (dashed red circle in Figure 1a), permitting identification of the flood already when it had reached the town of Rech, 6 km, or almost 1.5 hr flow time upstream of Walporzheim. By combining data from several stations, for example, station AHRW and the hypothetical station 2 km to the southwest, additional and more robust information could be provided on flood location, velocity, water level and hence inundated cross-sectional area, and debris flux. With at least three stations registering a flood signal, the location of the seismic source can be determined

in time-resolved manner by several independent techniques (Cook et al., 2021). Based on such location estimates, flood propagation speed could be constrained with sufficient confidence that false alarms would be minimal.

While national seismometer networks, typically configured for earthquake detection, can be used for flood sensing, they must be complemented with additional telemetric stations, not only to fill gaps but also to occupy landscape positions optimal for flood detection and quantification. Effective network densification could be pursued with low cost sensor systems (Manconi et al., 2018) that effectively cover the relevant frequency and sensitivity range of river flood signals. With ever cheaper instruments of adequate quality, and capability of live data streaming and near real time processing, denser seismic networks with autonomous power and data transmission have the potential to provide essential early warning information for many currently ungauged or insufficiently gauged upland catchments.

Functioning flood detection networks require robust workflows applying predefined processing routines such as the ones tested here for the 2021 Ahrtal flood. In this development, there is an important role for machine learning. This is straightforward where events are comparatively frequent and sufficiently similar in evolution (Beroza et al., 2021; Dammeier et al., 2016; Hibert et al., 2019). However, fast moving upland floods are rare events, for which seismic data is scarce. This curtails the training of the approach (Lemaître et al., 2017), adding to the difficulties arising when transferring a trained model from one study region to another (Hibert et al., 2019). In the light of these current limitations we favor seismic flood detection with classic rule-based methods. The parameters in our Ahrtal analysis are in most cases independent, so that false alarms can be suppressed by setting a threshold number of independent indicators for flood identification. Moreover, rules can be calibrated on site using smaller events.

Almost 10% of Europe's surface area consists of upland catchments that are potentially prone to rapidly evolving floods. This area is even less (1.3%) when applying high resolution process-based flood models (EEA, 2022) to identify landscape elements under direct threat of inundation. Medium sized upland catchments with valley-confined rivers, like the Ahrtal, could be instrumented with two or three “gate keeper” seismic station pairs (yellow and white stars in Figure 1a). Following this approach, all flood endangered European landscapes could be equipped with live telemetric seismic stations at a fraction (0.006%) of the costs caused by the Ahr flood in July 2021. Such a distributed network would systematically allow for several hours lead time to inform inhabitants of impending floods, and help optimize rapid response and rescue activities.

Data Availability Statement

All analyses were conducted in R v.0.4.1 using the packages terra (Hijmans, 2022), sp (Bivand et al., 2013), fields (Douglas et al., 2021), caTools (Tuszynski, 2021), and eisei (Dietze, 2022). The Supporting Information S1 contain a step by step code documentation of all workflows employed in this study. All figures and plots of the article are also generated in the Supporting Information S1 so that they can be fully reproduced. Only freely available data sets and software were used, as indicated by the corresponding references.

References

- Bell, R., Kron, W., Thiebes, B., & Thieken, A. (2022). Die Flutkatastrophe im Juli 2021 in Deutschland. Ein Jahr danach: Aufarbeitung und erste Lehren für die Zukunft, *Die Flutkatastrophe im Juli 2021 in Deutschland*, (Vol. 62, pp. 14–44). DKKV.
- Beroza, G., Segou, M., & Mouvasi, S. (2021). Machine learning and earthquake forecasting—Next steps. *Nature Communications*, 12(1), 4761. <https://doi.org/10.1038/s41467-021-24952-6>
- Bivand, R. S., Pebesma, E., & Gomez-Rubio, V. (2013). *Applied spatial data analysis with R* (2nd ed.). Springer. Retrieved from <https://asdar-book.org/>
- Burtin, A., Hovius, N., & Turowski, J. (2016). Seismic monitoring of torrential and fluvial processes. *Earth Surface Dynamics*, 4(2), 285–307. <https://doi.org/10.5194/esurf-4-285-2016>
- Chmiel, M., Godano, M., Piantini, M., Brigode, P., Gimbert, F., Bakker, M., et al. (2022). Brief communication: Seismological analysis of flood dynamics and hydrologically triggered earthquake swarms associated with storm Alex. *Natural Hazards and Earth System Sciences*, 22(5), 1541–1558. <https://doi.org/10.5194/nhess-22-1541-2022>
- Cook, K., Andermann, C., Gimbert, F., Adhikari, B. R., & Hovius, N., & Hovius, N. (2018). Glacial lake outburst floods as drivers of fluvial erosion in the Himalaya. *Science*, 362(6410), 53–57. <https://doi.org/10.1126/science.aat4981>
- Cook, K., Rekapalli, R., Dietze, M., Pilz, M., Cesca, S., Purnachandra, R., et al. (2021). Early warning of catastrophic flow events using regional seismic networks. *Science*, 374(6563), 87–92. <https://doi.org/10.1126/science.abj1227>
- Coviello, V., Capra, L., Vázquez, R., & Márquez-Ramírez, V. (2018). Seismic characterization of hyperconcentrated flows in a volcanic environment. *ESPL*, 43(10), 2219–2231. <https://doi.org/10.1002/esp.4387>

Acknowledgments

This research was supported by the HART (Hazard and Risk Team) action of Eifel Flood Event 2021 funded by the Helmholtz Centre Potsdam—GFZ German Research Centre for Geosciences and the DFG (German Research Foundation) Research Training Group Nat Risk Change—Natural Hazards and Risks in a Changing World. Open Access funding enabled and organized by Projekt DEAL.

- Dammeier, F., Moore, J., Hammer, C., Haslinger, F., & Loew, S. (2016). Automatic detection of alpine rockslides in continuous seismic data using hidden Markov models. *Journal of Geophysical Research: Earth Surface*, *121*(2), 351–371. <https://doi.org/10.1002/2015JF003647>
- Dietze, M. (2022). eSeis: Environmental seismology toolbox [Computer software manual]. R package version 0.7.0, Retrieved from <https://creativecommons.org/licenses/by/4.0/>
- Dietze, M., Bell, R., Ozturk, U., Cook, K. L., Andermann, C., Beer, A. R., et al. (2022). More than heavy rain turning into fast-flowing water—A landscape perspective on the 2021 Eifel floods. *Natural Hazards and Earth System Sciences*, *22*(6), 1845–1856. <https://doi.org/10.5194/nhess-22-1845-2022>
- Dietze, M., Lagarde, S., Halfi, E., Laronne, J., & Turowski, J. (2019). Joint sensing of bedload flux and water depth by seismic data inversion. *Water Resources Research*, *55*(11), 9892–9904. <https://doi.org/10.1029/2019WR026072>
- Dietze, M., & Ozturk, U. (2021). A flood of disaster response challenges. *Science*, *373*(6561), 1317–1318. <https://doi.org/10.1126/science.abm0617>
- Douglas, N., Furrer, R., Paige, J., & Sain, S. (2021). Fields: Tools for spatial data. R package version 13.3. Retrieved from <https://github.com/dnchka/fieldsRPackage>
- EEA. (2022). European environment agency. Retrieved from <https://sdi.eea.europa.eu/>
- Eibl, E., Bean, C., Einarsson, B., Palsson, F., & Vogjörd, K. (2017). Seismic ground vibrations give advanced early-warning of subglacial floods. *Nature Communications*, *11*(1), 2504. <https://doi.org/10.1038/s41467-020-15744-5>
- Gimbert, F., Tsai, V., & Lamb, M. (2014). A physical model for seismic noise generation by turbulent flow in rivers. *Journal of Geophysical Research*, *119*(10), 2209–2238. <https://doi.org/10.1002/2014JF003201>
- Gocht, M., Schröter, K., Ostrowski, M., Rubin, C., & Nachtnebel, H. (2009). In *Flood risk management: Research and practice*. In P. Samuels, S. Huntington, W. Allsop, & J. Harrop (Eds.), Taylor & Francis Group.
- Goodling, P. J., Lekic, V., & Prestegard, K. (2018). Seismic signature of turbulence during the 2017 Oroville dam spillway erosion crisis. *Earth Surface Dynamics*, *6*(2), 351–367. <https://doi.org/10.5194/esurf-6-351-2018>
- Hibert, C., Michea, D., Provost, F., Malet, J., & Geertsema, M. (2019). Exploration of continuous seismic recordings with a machine learning approach to document 20 yr of landslide activity in Alaska. *Geophysical Journal International*, *219*(2), 1138–1147. <https://doi.org/10.1093/gji/ggz354>
- Hijmans, R. J. (2022). Terra: Spatial data analysis [Computer software manual]. R package version 1.5-34, Retrieved from <https://CRAN.R-project.org/package=terra>
- HRC. (2007). Global flash flood guidance program. Retrieved from <https://www.hrcwater.org/projects/project-1/2022-06-28>
- IPCC. (2018). Global warming of 1.5°C. An IPCC special report on the impacts of global warming of 1.5°C above pre-industrial levels and related global greenhouse gas emission pathways. In *The context of strengthening the global response to the threat of climate change, sustainable development, and efforts to eradicate poverty*, In V. Masson-Delmotte (Ed.). Cambridge University Press.
- Junghänel, T., Bissolli, P., Dassler, J., Fleckenstein, R., Imbery, F., Janssen, W., et al. (2021). *Hydro-klimatologische Einordnung der Stark- und Dauerniederschläge in Teilen Deutschlands im Zusammenhang mit dem Tiefdruckgebiet Bernd vom 12. bis 19.* Report DWD German Weather Bureau. Retrieved from https://www.dwd.de/DE/leistungen/besondereereignisse/niederschlag/20210721/_bericht/_starkniederschlaege/_tief/_bernd.pdf?__blob=publicationFile&v=6
- Kreibich, H., Piroth, K., Seifert, I., Maiwald, H., Kunert, U., Schwarz, J., et al. (2009). Is flow velocity a significant parameter in flood damage modelling? *Natural Hazards and Earth System Sciences*, *9*(5), 1679–1692. <https://doi.org/10.5194/nhess-9-1679-2009>
- Lemaître, G., Nogueira, F., & Aridas, C. (2017). Imbalanced-learn: A python toolbox to tackle the curse of imbalanced datasets in machine learning. *Journal of Machine Learning Research*, *18*, 1–5. <https://doi.org/10.5555/3122009.3122026>
- Manconi, A., Coviello, V., Galletti, M., & Seifert, R. (2018). Short communication: Monitoring rockfalls with the raspberry shake. *Earth Surface Dynamics*, *6*(4), 1219–1227. <https://doi.org/10.5194/esurf-6-1219-2018>
- Nikogosian, C., Winterrath, T., Walawander, E., Fischer, I., Schmitz-Kröll, D., & Wischott, V. (2021). *Klassifikation meteorologischer Extremereignisse zur Risikoversorge gegenüber Starkregen für den Bevölkerungsschutz und die Stadtentwicklung*. Abschlussbericht. Retrieved from https://www.dwd.de/DE/fachnutzer/wasserrwirtschaft/kooperationen/klamex/pdf/abschlussbericht/_klamex.pdf?__blob=publicationFile&v=5
- Polvi, L., Dietze, M., Lotsari, E., Turowski, J., & Lind, L. (2020). Seismic monitoring of a subarctic river: Seasonal variations in hydraulics, sediment transport, and ice dynamics. *Journal of Geophysical Research: Earth Surface*, *125*(7), e2019JF005333. <https://doi.org/10.1029/2019JF005333>
- Roggenkamp, T., & Herget, J. (2022). Hochwasser der ahr im juli 2021—abflussabschätzung und einordnung. *Hydrologische Notizen*, *66*, 40–49.
- Schneiderbauer, S., Fontanella Pisa, P., Delves, J. L., Pedoth, L., Rufat, S., Erschbamer, M., et al. (2021). Risk perception of climate change and natural hazards in global mountain regions: A critical review. *Science of the Total Environment*, *784*, 146957. <https://doi.org/10.1016/j.scitotenv.2021.146957>
- Tsai, V., Minchew, B., Lamb, M. P., & Ampuero, J.-P. (2012). A physical model for seismic noise generation from sediment transport in rivers. *Geophysical Research Letters*, *39*(2), L02404. <https://doi.org/10.1029/2011GL050255>
- Tuszynski, J. (2021). Catools: Tools: Moving window statistics, gif, base64, roc auc, etc [Computer software manual]. R package version 1.18.2. Retrieved from <https://CRAN.R-project.org/package=caTools>
- Walter, F., Burtin, A., McArdell, B., Hovius, N., Weder, B., & Turowski, J. (2017). Testing seismic amplitude source location for fast debris-flow detection at Illgraben, Switzerland. *Natural Hazards and Earth System Sciences*, *17*(6), 939–955. <https://doi.org/10.5194/nhess-17-939-2017>
- Wong, M., & Parker, G. (2006). Reanalysis and correction of bed-load relation of Meyer-Peter and Müller using their own database. *Journal of Hydrologic Engineering*, *13*(2), 1159–1168. [https://doi.org/10.1061/\(ASCE\)0733-9429](https://doi.org/10.1061/(ASCE)0733-9429)
- Yang, C.-F., Chi, W.-C., & Lai, Y.-J. (2018). Seismically detected ground tilts induced by precipitation and fluvial processes: An example from Taiwan. *Journal of Geophysical Research: Solid Earth*, *123*(6), 4814–4828. <https://doi.org/10.1029/2017JB014768>